Helmholtz-Zentrum
Geesthacht
Zentrum für Material- und Küstenforschung

Final Draft
of the original manuscript:

Okulov, I.V.; Lamaka, S.V.; Wada, T.; Yubuta, K.; Zheludkevich, M.L.;
Weissmueller, J.; Markmann, J.; Kato, H.:

Nanoporous magnesium

In: Nano Research (2018) Springer

DOI: 10.1007/s12274-018-2167-9

Nanoporous Magnesium

I.V. Okulov[a,b,*], S.V. Lamaka[c], T. Wada[a], K. Yubuta[a], , M.L. Zheludkevich[c,d], J. Weissmüller[b,e], J. Markmann[b,e] and H. Kato[a]

[a]Tohoku University, Institute for Materials Research, Katahira 2-1-1, Sendai 980-8577, Japan
[b]Helmholtz-Zentrum Geesthacht, Institute of Materials Research, Materials Mechanics, Geesthacht, Germany
[c]Helmholtz-Zentrum Geesthacht, MagIC—Magnesium Innovation Centre, Geesthacht, Germany
[d]University of Kiel, Faculty of Engineering, Kiel, Germany
[e]Hamburg University of Technology, Institute of Materials Physics and Technology, Hamburg, Germany

*Corresponding author; E-mail: okulovilya@yandex.ru and ilya.okulov@hzg.de

Keywords: Dealloying; Nanoporous; Magnesium.

Abstract

In our study, we present freestanding nanoporous magnesium (Mg) as a novel material: a lightweight metal even less dense due to its porosity with potential for structural and functional applications. Until now, the high reactivity of Mg with oxygen and aqueous media prevented fabrication of nanoporous Mg. Firstly, in order to synthesize nanoporous Mg, we fabricated a bicontinuous nanocomposite consisting of interpenetrating Mg and non-Mg phases by liquid metal dealloying. The non-Mg phases in the nanocomposite protects Mg against corrosion. Secondly, we etched the non-Mg phases from the nanocomposite leaving nanoporous Mg by HF solution. This works because the nanoporous Mg was passivated by a MgF_2 layer during the etching. Our approach is very flexible and we demonstrate that versatile microstructures of the nanoporous Mg – e.g. nanoscale bicontinuous network or hierarchical or plate-like structures, etc. – can be designed upon given needs. More importantly, these nanoporous Mg samples can readily be exposed to air without taking harm by corrosion.

Dealloyed nanoporous materials take form of macroscopic bodies, consisting of a network of nanosized struts [1–3]. As the distinguishing features, the large specific surface area and small size of each single nanoscale object result in surface- and size-controlled properties. These properties are transferred to the macroscopic material resulting in improved or entirely new materials behavior for applications in catalysis [4], actuation [5], and energy storage and conversion [6]. The standard synthesis schemes of nanoporous metals by dealloying employ corrosion in aqueous solutions and can supply only nanoporous noble or coinage metals such as Au [7], Ag [8], Pd [9] or Ni [10]. Less noble and more affordable as well as lighter nanoporous metals, such as stainless steel [11], and titanium alloys [12–15], can be prepared by corrosion in liquid metal [16]. There would be a high interest in making nanoporous Mg (npMg), since Mg is abundant (hence low cost) and light-weight and since it has important applications in storing hydrogen [17], as an anode material [18] and as a biomaterial that can be resorbed [19]. Yet, the high reactivity of Mg with oxygen and aqueous media has so far prevented the synthesis of npMg. Here, we demonstrate that liquid metal corrosion approach can be modified to supply npMg. The key to achieving stability of npMg is passivation by a superficial layer of MgF_2. The versatility of our approach is demonstrated by npMg samples with diverse microstructures including nanoscale network structures as well as plate-like, grid-like, and hierarchical porous scaffolds.

Nanoporous materials synthesized by dealloying are a great example of a strategy to assemble many (10^{18} for 1 cm^3 of material with a 10 nm structure size) nanoscale objects into a macroscopic body. The intrinsic size effect of these nanoscale objects is inherited by nanoporous materials and often leads to increasing of their strength with decreasing dimension of structural units as it was demonstrated for nanoporous gold [20,21]. A decisive advance on the way to technologically relevant nanoporous materials for structural applications would be nanoporous scaffolds consisting of Mg as one of the most abundant and lightweight metal. More importantly, npMg can serve as functional material, e.g. for energy storage [18,22] and in medicine [19]. Anodes with high energy density and high-rate performance can be based on micro-/nanostructured Mg material in form of microspheres, microplates, and nanorods [22]. Since even smaller structures promise shorter transport distances and hence further improved kinetics, Mg electrodes with a well-interconnected network *at the nanoscale* in form of freestanding nanoporous material is desired for the battery application.

However, porous Mg so far has a structure size of a few tens of micrometers or more,[23] whereas npMg has not been reported.

This work reports on the preparation of nanoporous Mg. As described in Materials and Methods, a number of $Ti_{50-x}(Nb, Ta, V, Fe)_xCu_{50}$ precursor alloys was designed for synthesis of the open porous Mg with various morphologies by liquid metal dealloying. Liquid metal dealloying is a variant of dealloying where the corrosive medium is a liquid metal [16,24,25]. Our approach involves selective dissolution of Cu leaving behind porous $Ti_{50-x}(Nb, Ta, V, Fe)_x$ scaffolds surrounded by liquid Mg. The as-dealloyed samples are cooled down what leads to solidification of Mg in the pore space of the $Ti_{50-x}(Nb, Ta, V, Fe)_x$ scaffolds. Subsequently, the non-Mg phases are etched in an aqueous medium while Mg remains. This yields npMg.

This approach is now demonstrated based on the example of the $Ti_{41}Ta_9Cu_{50}$ precursor alloy. $Ti_{41}Ta_9Cu_{50}$ was dealloyed in liquid Mg at 1073 K for 20 min in order to obtain a composite microstructure consisting of non-Mg and Mg phases (Fig. 1 a). Scanning electron microscopy (SEM) of the material in its as-dealloyed state – i.e. after corrosion in liquid Mg but prior to the subsequent etching in HF – reveals a dendritic morphology (Fig. 1 a). The dendrites exhibit a core-shell structure, with Energy-dispersive x-ray spectroscopy (EDX) indicating a Ta-rich core and Ti-rich phase shell. The SEM shows a Ti-rich and a Mg-rich phase in the the matrix surrounding the dendrites (Fig. 1). X-ray diffraction data indicates three different phases (Fig. 1 a), namely bcc Ta, hcp Ti, and hcp Mg. According to X-ray analysis, the as-dealloyed sample consists of three different phases (Fig. 1 a). Together, the three techniques show that the dendrite core consists of the bcc solid solution of Ti and Cu in Ta, that the dendrite shell consists of the hcp Ti(Ta, Cu) solid solution phase and that the matrix surrounding dendrites is a mixture of hcp Ti(Ta) and hcp Mg phases.

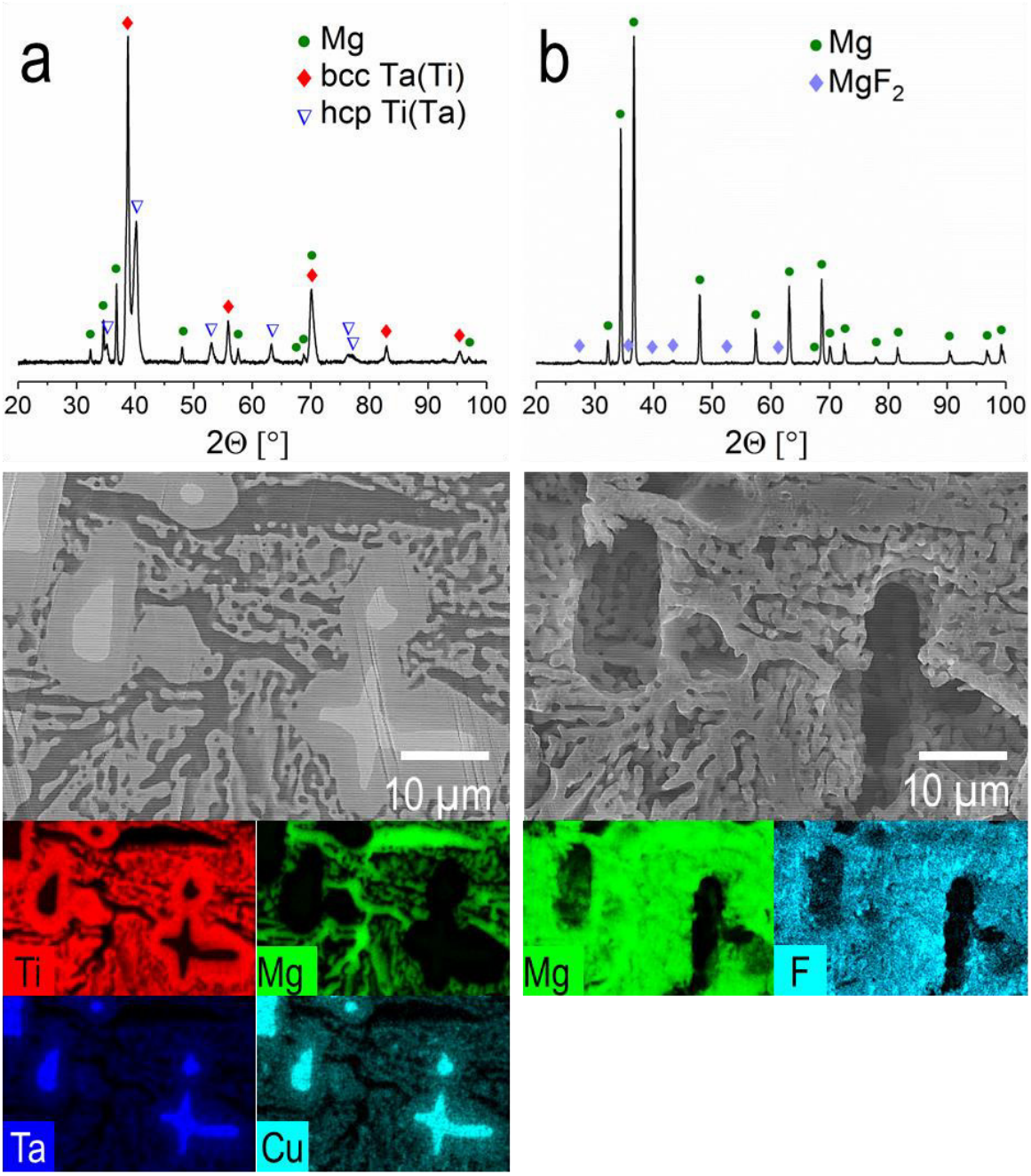

Figure 1 Microstructure of the as-dealloyed $Ti_{41}Ta_9Cu_{50}$ precursor alloy before (a) and after etching (b) in 15 M HF solution. (a) X-Ray diffraction pattern, scanning electron micrograph, and elemental mappings of the as-dealloyed $Ti_{41}Ta_9Cu_{50}$ before etching; (b) X-Ray diffraction pattern, scanning electron micrograph, and elemental mappings of the as-dealloyed $Ti_{41}Ta_9Cu_{50}$ after etching. The same place is shown before and after etching. Fig. 1 b reveals hierarchically structured open porous Mg.

Fig. 1 b shows data analogous to Fig. 1 a, but after exposing the as-dealloyed sample to a 15M aqueous solution of HF. It is seen that this leads to etching of the non-Mg phases, hcp Ti and bcc Ta. Remarkably, the Mg does not dissolve in HF. The figure shows that the resulting Mg has an open porous structure with two structural length scales (or hierarchy levels). Comparison to Fig. 1 a reveals that the larger pores (several tens of µm in size) represent etched dendrites while the smaller pores (few µm in size) represent the etched Ti-rich phase from the matrix. Comparison of Fig. 1 a and Fig. 1 b indicates further that the morphology of the Mg phase remains unchanged. The data in Fig. 1 a and b clearly demonstrate that our combination of liquid-Mg dealloying followed by etching in HF yields porous Mg.

The passivation of Mg in hydrofluoric acid has been linked to the formation of a dense layer of MgF_2 [26]. The X-ray analysis in Fig. 1 b shows the presence of hcp Mg and confirms tetragonal MgF_2 phase as a second phase of our porous Mg. Additionally, the EDX analysis of the porous Mg sample reveals presence of about 83,8 at.% of Mg, 14.5 at.% of F and some traces of Cu dissolved in Mg. Besides passivating Mg against corrosion, the magnesium fluoride layer also stabilizes Mg in air by reducing the oxidation rate [19].

The passivation layer was further investigated by inspection of a milled cross-section of npMg by focused ion beam (FIB) (Fig. 2). The surface of npMg shown in Fig. 4 b was milled at 0 ˚ to the ion beam and then tilted to 90 ˚ to the electron beam. The SEM of Fig. 2 shows a Mg ligament covered by a layer, about 200 nm thick, of different contrast. The origin of the pores in the ligament will be discussed later. EDX finds Mg, F, O and Ga in the layer. The Ga is readily attributed to the FIB milling. The presence of O atoms can be explained by presence of the $MgF_{2-x}OH_x{\cdot}yH_2O$ phase. Some F^- ions can be replaced by hydroxyl (OH^-) ions in the MgF_2 structure forming $MgF_{2-x}OH_x{\cdot}yH_2O$ [26]. The lack of its reflections in the X-ray diffractogram might mean that this is amorphous. Only Mg is found in the center of the ligament.

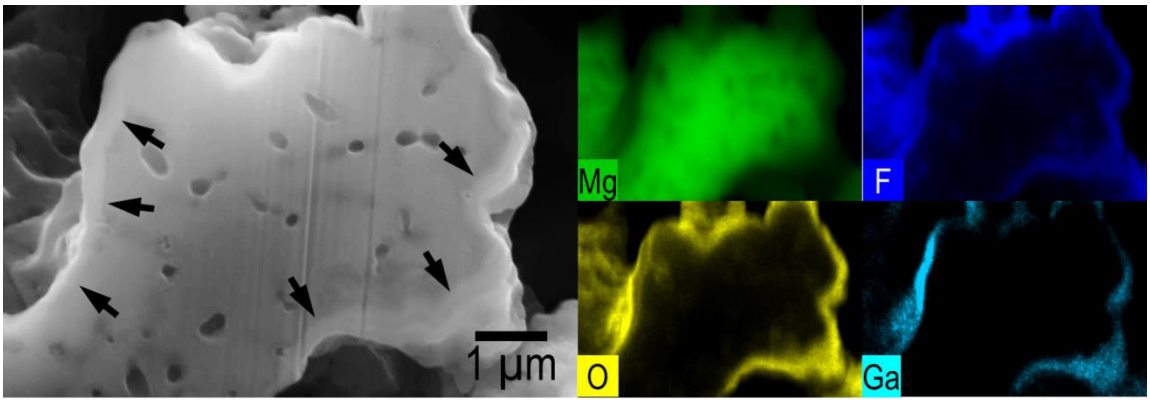

Figure 2 Microstructure and elemental mappings of a ligament in open porous Mg. The sample is made by dealloying of the $Ti_{50}Cu_{50}$ precursor alloy (2 mm rod) at 1073 K for 20 min following by 30 min etching in a 15 M HF solution. The observed surface was milled by focused ion beam (FIB). The arrows indicate the border of the layer covering the magnesium ligament.

The following paragraphs demonstrate that microstructure of porous Mg can be tuned through classical metallurgical approaches and by varying the parameters of the liquid metal dealloying. In this series of examples, the first one is related to the "classical" approach, namely varying microstructure of the precursor alloy by applying different cooling rates. Figs. 3 a and b show microstructures of npMg synthesized from the same $Ti_{38.75}Nb_{11.25}Cu_{50}$ precursor alloy fabricated at different cooling rates. Particularly, Figs. 3 a displays the hierarchically structured npMg obtained by dealloying of a 6 mm plate $Ti_{38.75}Nb_{11.25}Cu_{50}$ sample. Due to the immiscibility of Nb and Cu, the primary Ti(Nb) dendrites formed upon solidification of the $Ti_{38.75}Nb_{11.25}Cu_{50}$ alloy like it was reported for the titanium alloys with a similar chemical composition [27–29]. This is, in fact, similar to the above described $Ti_{41}Ta_9Cu_{50}$ alloy case. The dendrites of the $Ti_{38.75}Nb_{11.25}Cu_{50}$ sample mainly consist of Ti and Nb and, therefore, remained untouched by liquid Mg during liquid metal dealloying. The immersion of the as-dealloyed $Ti_{38.75}Nb_{11.25}Cu_{50}$ alloy sample into the HF solution led to etching of these Ti(Nb) dendrites and the Ti-rich matrix phase leaving porous Mg covered by a MgF_2-rich layer. Eventually, the open porous Mg exhibits a hierarchical structure.

The microstructure of the porous Mg is strongly affected by the solidification rate of the $Ti_{38.75}Nb_{11.25}Cu_{50}$ precursor alloy. Rapid solidification was here realized by melt-spinning, which reaches cooling rates around 10^3 K s^{-1} [30], several orders of magnitude higher compared to that of the 6 mm plate. The primary Nb-rich dendrites do not form at the high cooling rate of melt spinning.

This is apparent in Fig. 3 b, which shows the corresponding npMg microstructure. The network of homogenously interconnected ligaments resembles that of nanoporous gold. The ligament size is 60 ± 14 nm.

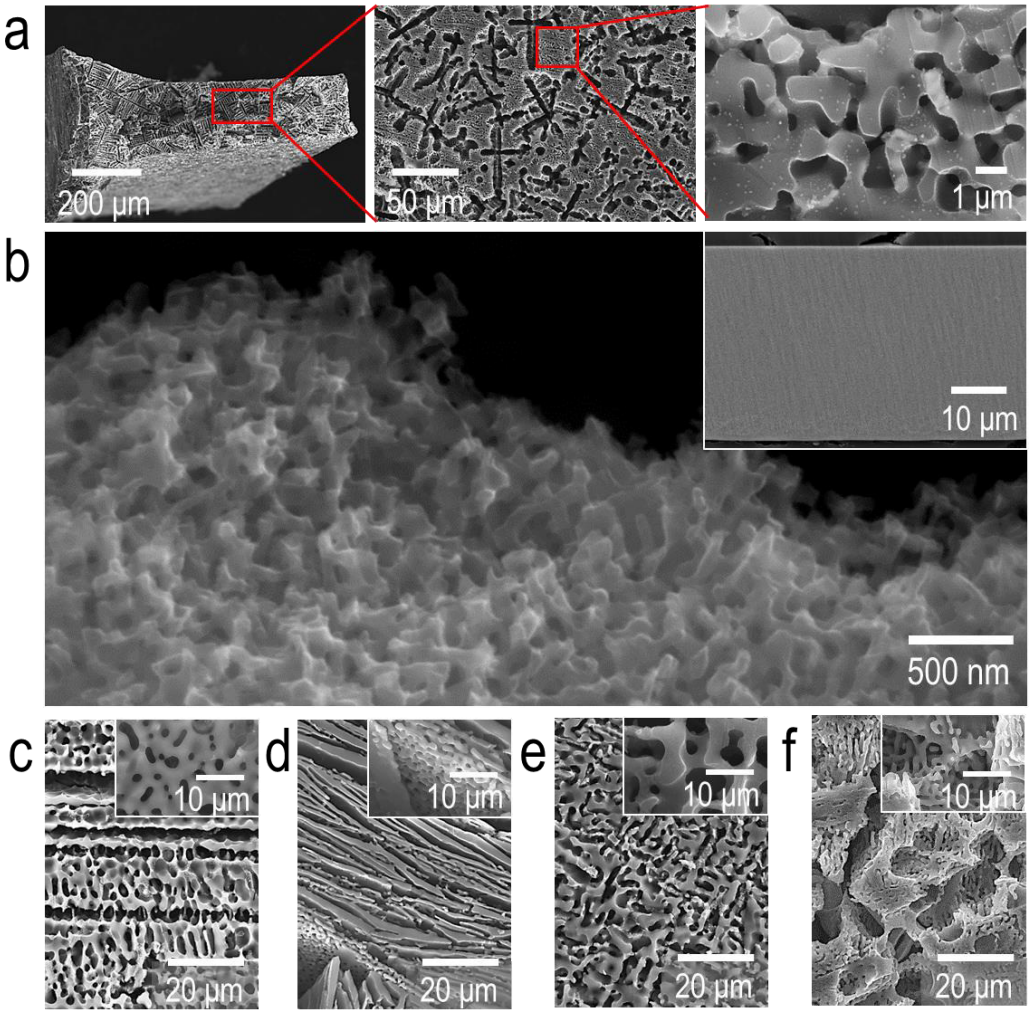

Figure 3 Tuning microstructure of the open porous Mg through optimization of the precursor alloy microstructure. Secondary electron micrographs of porous Mg fabricated from: (a) 6 mm plate of $Ti_{38.75}Nb_{11.25}Cu_{50}$; (b) melt-spun ribbon of $Ti_{38.75}Nb_{11.25}Cu_{50}$ dealloyed at 973 K for 30 s (inset: ion-milled cross-section of the as-dealloyed ribbon showing its homogeneous microstructure); (c) 6 mm plate of $Ti_{50}Cu_{50}$; (d) 6 mm plate of $Ti_{42.5}V_{7.5}Cu_{50}$; (e) 6 mm plate of $Ti_{40}Fe_{10}Cu_{50}$; and (f) as arc-melted $Ti_{41}Ta_9Cu_{50}$ sample. Insets in c-d correspond to secondary electron micrographs of the porous Mg taken at a higher magnification. The $Ti_{38.75}Nb_{11.25}Cu_{50}$, $Ti_{50}Cu_{50}$, $Ti_{42.5}V_{7.5}Cu_{50}$, $Ti_{40}Fe_{10}Cu_{50}$, and $Ti_{41}Ta_9Cu_{50}$ samples were dealloyed at 1073 K for 20 min.

Besides variation of cooling rates, the microstructure of the precursor alloy also can be tailored by alloying. Figs. 3 a and d-f display diverse morphologies of npMg, such as plate-like, grid-like or hierarchically structured ones, synthesized from the different precursor alloys but under identical dealloying conditions. These precursor alloys were fabricated based on the $Ti_{50}Cu_{50}$ alloy. The Ti element was partially substituted by the elements stabilizing β-Ti, such as V, Fe, Nb and Ta [31–34]. These elements are immiscible with Cu at room temperature [35]. Therefore, primary dendrites precipitate in the as-cast $Ti_{38.75}Nb_{11.25}Cu_{50}$ and $Ti_{41}Ta_9Cu_{50}$ (Figs. 1 and 3 a and f), leading to dendritic-shaped pores in the corresponding npMg samples. The microstructure of npMg obtained from the $Ti_{50}Cu_{50}$ sample (Fig. 3 c) is notably different as compared to the above npMg samples. It consists of connected porous plates as exemplified in Fig. 3 c inset. This reflects the microstructure effect of the as-cast $Ti_{50}Cu_{50}$ precursor alloy samples. A plate-like structure was also observed for the npMg samples obtained from the $Ti_{42.5}V_{7.5}Cu_{50}$ sample. As in the $Ti_{50}Cu_{50}$ case, the Mg plate structures in the $Ti_{42.5}V_{7.5}Cu_{50}$-based npMg sample possess an internal porous structure (Fig. 3 d inset). The microstructure of these plate structures formed during dealloying in liquid Mg and became porous after subsequent etching of the non-Mg phases. The grid-like morphology can be designed by alloying of the $Ti_{50}Cu_{50}$ alloy with Fe (Fig. 3 e). These examples demonstrate the importance of alloying for tuning the microstructure of the final npMg sample [36].

Figs. 4 a and b show that the npMg microstructure can be tuned not only by optimizing the microstructure of the precursor alloy by alloying or fabrication method but also by varying dealloying conditions. The $Ti_{50}Cu_{50}$ samples were dealloyed applying different dealloying time and temperature to obtain hierarchical npMg samples. Reducing dealloying time and temperature leads to significant reduction of the porosity size (both large and small) while keeping the hierarchical structure (Figs. 4 a and b). Particularly, the size of the large pores reduced from a few microns to a few hundreds of nanometers. The small pores follow a similar trend, namely their size reduces from about 160 nm (Fig. 4 a, inset) to 20 nm (Fig. 4 b, inset). The morphology of these small spherical pores is acquired from the shape of the titanium-rich phase formed upon dealloying of the $Ti_{50}Cu_{50}$ alloy. Evidence for that conclusion is demonstrated in the inset of Fig. 4 b displaying the porous Ti obtained from as-dealloyed $Ti_{50}Cu_{50}$ alloy by the standard procedure of etching the Mg phase out of the as-dealloyed composite with nitric acid [16,37]. Indeed, the titanium phase is covered by spherical particles of the same size and shape as the small spherical pores covering the ligaments of npMg.

Tuning the pore size of npMg is possible not only by variation of dealloying conditions but also through variation of the chemical composition of the precursor alloys as it is shown below.

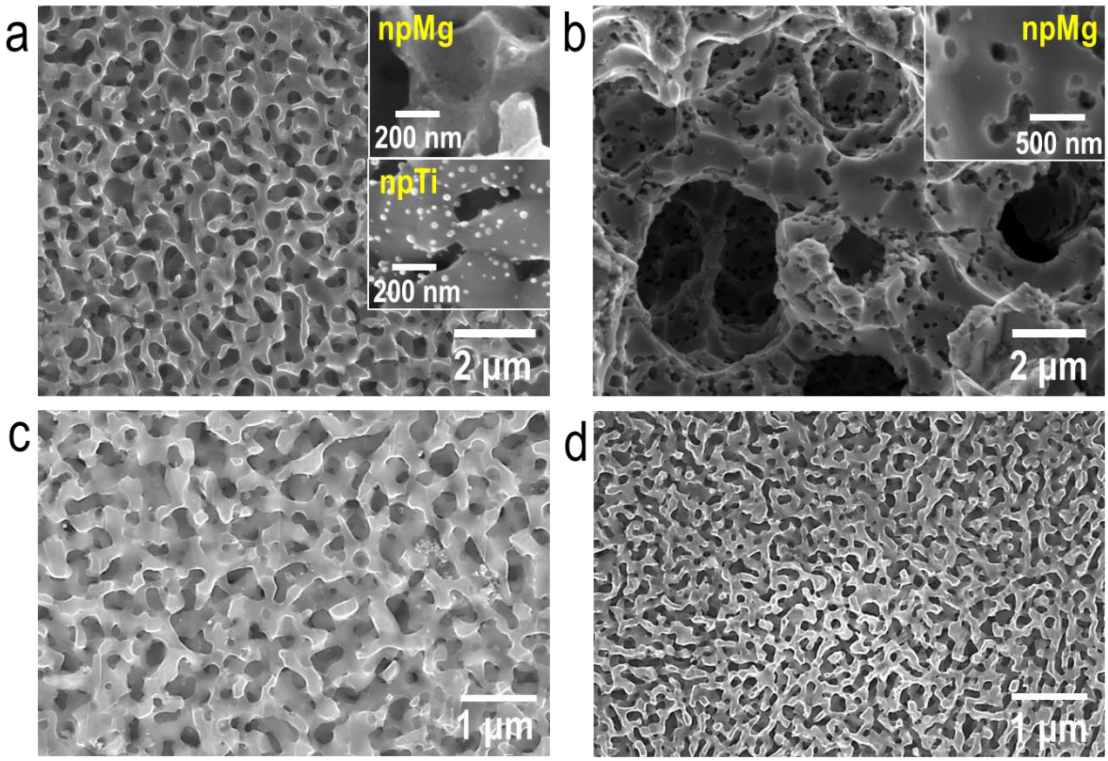

Figure 4Tuning microstructure of the open porous Mg through varying dealloying conditions (a and b) and alloying (c and d). The porous Mg fabricated from: (a) 2 mm rod of $Ti_{50}Cu_{50}$ dealloyed at 1073 K for 20min; (b) ribbon of $Ti_{50}Cu_{50}$ sample dealloyed at 973 K for 1 min; (c) ribbon of $Ti_{40}Fe_{10}Cu_{50}$ dealloyed at 973 K for 30 s; and (d) ribbon of $Ti_{38.75}Nb_{11.25}Cu_{50}$ dealloyed at 973 K for 30 s. Insets in "a" are the nanoporous Mg (upper) and the nanoporous Ti (lower). Inset in "b" is an image of the same nanoporous Mg at higher magnification.

Figs. 4 c and d discloses an interesting approach to refine microstructure of the nanoporous Mg through alloying of precursor alloys by high melting point elements. In the current case, the $Ti_{40}Fe_{10}Cu_{50}$ and $Ti_{38.75}Nb_{11.25}Cu_{50}$ alloys were designed by modification of the parent $Ti_{50}Cu_{50}$ alloy through partial substitution of Ti by Fe or Nb. These alloys were melt-spun into ribbon shape and dealloyed under identical conditions. The microstructure of the resulting npMg samples is shown in Figs. 4 c and d. The ligament size of npMg from the $Ti_{38.75}Nb_{11.25}Cu_{50}$ alloy (about 60 nm) is about two times finer as compared to npMg from the $Ti_{40}Fe_{10}Cu_{50}$ alloy (about 124 nm). This is due to the higher melting point of Nb as compared to that of Fe. Since the liquid metal dealloying is a diffusion-

mediated process [25], alloying by elements possessing higher melting point leads to a lower diffusion rate during dealloying and, therefore, a finer microstructure of the as-dealloyed materials [38].

Thus, our results pave the way for the design of npMg-based materials fulfilling requirements for different application fields: lightweight structures, bioabsorbable implant scaffolds, battery anode materials, hydrogen storage materials, drug delivery structures. Particularly, we anticipate our results to advance energy storage by using npMg electrodes since Mg possesses higher volumetric capacities than lithium, it is safer (e.g. no dendritic formation during plating/stripping) and more abundant in the earth crust than lithium [18,39]. As for biomedical applications, "*in vitro* and *in vivo* studies suggest that Mg promotes osteoblast proliferation, differentiation and expression of osteogenic markers and, moreover, porous Mg can safely degrade in endosseous sites inducing new bone formation and stimulating angiogenesis" [19].

Therefore, design of bioinspired hierarchical porous Mg structures similar to bone seems to be promising for bone trauma healing. Especially for this kind of applications, polymer infiltration of such scaffolds might be an option for improvement of their load-bearing performance [37,40].

In summary, we presented open nanoporous Mg synthesized by dealloying of Ti(Me)Cu-based alloys (Me = Fe, V, Nb, Ta) in liquid Mg followed by etching out the non-Mg phases from the as-dealloyed samples by subjection to 15 M HF. During the latter corrosion step, the surface of npMg passivates by developing a MgF_2-rich layer preventing rapid oxidation of the porous samples. The pore size of the presented npMg ranges from about 20 nm up to 9.4 µm. Our synthesis approach allows fabrication of diverse structures of npMg including hierarchical ones. The developed npMg samples possess well-interconnected and freestanding structure. The tunable microstructure of npMg can be optimized upon given needs by using the following tools: adjustment of dealloying conditions, i.e. time and temperature; variation of the chemical composition of the precursor alloy, e.g. alloying the precursor by elements possessing high melting point for refinement of the npMg microstructure; and tailoring microstructure of the precursor alloy by optimization of fabrication conditions or/and by alloying, e.g. through the formation of dendrites in the initial alloy.

Materials and methods

The nanoporous Mg was fabricated in a two-step process. Firstly, the $Ti(Nb, Ta, V, Fe)_{50}Cu_{50}$ alloys were dealloyed in liquid Mg in order to synthesize interpenetrating-phase composites. These composites mainly consist of Ti-rich and Mg-rich phases. Secondly, the Ti-rich phase was etched by selective dissolution in 15 M aqueous solution of HF for several minutes in an ultrasonic bath following by cleaning in deionized water and alcohol. The detailed experimental procedure is described below.

The initial $Ti_{50}Cu_{50}$, $Ti_{38.75}Nb_{11.25}Cu_{50}$, $Ti_{41}Ta_9Cu_{50}$, $Ti_{42.5}V_{7.5}Cu_{50}$, and $Ti_{40}Fe_{10}Cu_{50}$ precursor alloys were prepared from pure metals (99.9 %) by an arc melting device. The alloying elements like Nb, Ta, V, and Fe were selected because these are immiscible with Cu and, therefore, tend to form Ti(Nb, Ta, V, Fe) dendritic structures upon solidification at relatively low cooling rates. These precursor alloys were used for fabrication of samples for dealloying, i.e. ribbon shape samples by melt spinning, rod shape samples by injection casting and plate shape samples by casting. The fabrication of samples was conducted under argon atmosphere. The ribbons of 30-40 μm in thickness were fabricated from all alloys. The rod shaped samples were prepared from $Ti_{50}Cu_{50}$ (2 mm in diameter) and $Ti_{38.75}Nb_{11.25}Cu_{50}$, $Ti_{42.5}V_{7.5}Cu_{50}$ (1.5 mm in diameter). For the plate shaped samples, a copper mold with inner space of 6 x 30 x 70 mm^3 was used. Samples of 1 mm thickness were cut from these plates for dealloying. The 6 mm plate samples were fabricated from all alloys except $Ti_{41}Ta_9Cu_{50}$ for which as arc-melted samples were used for dealloying.

Table 1. Samples fabricated from the precursor alloys for this study.

Precursor alloy (at%)	As arc-melted	Ribbon	Rod (diameter)	Plate
$Ti_{50}Cu_{50}$	No	Yes	Yes (2 mm)	Yes
$Ti_{40}Fe_{10}Cu_{50}$	No	Yes	No	Yes
$Ti_{42.5}V_{7.5}Cu_{50}$	No	Yes	Yes (1.5 mm)	Yes

$Ti_{38.75}Nb_{11.25}Cu_{50}$	No	Yes	Yes (1.5 mm)	Yes
$Ti_{41}Ta_{9}Cu_{50}$	Yes	Yes	No	No

For the liquid metal dealloying, the plate and rod samples were immersed in Mg melt (99.99 %) at 1073 K for 20 min. The ribbon samples (30 - 50 μm in thickness) were immersed in Mg melt at 973 K for 30 s and 60 s. Generally, upon dealloying, molten Mg selectively dissolves the Cu-rich phase out of the parent alloys, while Ti(Nb, Ta, V, Fe) diffuses along the metal/liquid interface. However, in the case of precursor samples containing Ti(Nb, Ta, V, Fe) dendrites formed during solidification, e.g. for the 6 mm plate samples of $Ti_{38.75}Nb_{11.25}Cu_{50}$ or the arc-melted samples of $Ti_{41}Ta_{9}Cu_{50}$, the Ti(Nb, Ta), these dendrites remains untouched during the dealloying process. After dealloying, the samples, denominated here as Ti(Nb, Ta, V, Fe)-Mg interpenetrating-phase composites, consist of Ti-rich and Mg-rich phases.

Structural investigation was performed by X-ray diffraction in Bragg-Brentano geometry (Rigaku Ultima, Japan) with Cu-K_α radiation. Scanning electron microscopy (SEM, Karl Zeiss, Gemini Ultra 55, Germany) coupled with energy-dispersive X-ray analysis (Bruker, Germany) explored microstructure and composition. The surface of the samples for the SEM was prepared by Ar ion milling (E-3500, Hitachi, Japan) of a cross-sectional surface of the as-dealloyed composites. The non-Mg phases were etched in HF solution after the surface was milled. In the case of MgF_2-layer analysis, a cross-sectional image of porous Mg was obtained using a focused ion beam/scanning ion microscope system (FIB-SIM; JEOL JEM-9320FIB, Tokyo, Japan). The already porous Mg was milled at 0˚ to the ion beam and then tilted to 90˚ to the electron beam for SEM.

Supplementary information

Table 1 Pore size of different npMg samples synthesized in this study. Note: in case of the hierarchically structured npMg, the second value indicates the largest pore size (for $Ti_{50}Cu_{50}$), the distance between porous plates (for $Ti_{42.5}V_{7.5}Cu_{50}$) or the thickness of etched dendritic arms (for $Ti_{38.75}Nb_{11.25}Cu_{50}$ and $Ti_{41}Ta_9Cu_{50}$). The pore size is measured using SEM micrographs.

Precursor alloy (at%)	**Arc-melted**	**Ribbon**	**Rod**	**Plate**
$Ti_{50}Cu_{50}$	no sample	20 ± 2 nm and 253 ± 107 nm	0.16 ± 0.04 µm and 4.3 ± 1.2 µm	1.57 ± 0.46 µm
$Ti_{40}Fe_{10}Cu_{50}$	no sample	204 ± 53 nm	no sample	1.77 ± 0.63 µm
$Ti_{42.5}V_{7.5}Cu_{50}$	no sample	no sample	2.1 ± 0.7 µm	0.82 ± 0.16 µm and 2.9 ± 2.2 µm
$Ti_{38.75}Nb_{11.25}Cu_{50}$	no sample	70 ± 13 nm	1.19 ± 0.75 µm	0.49 ± 0.10 µm and 5.7 ± 1.3 µm
$Ti_{41}Ta_9Cu_{50}$	0.81 ± 0.28 µm and 9.4 ± 2.1 µm	60 ± 16 nm	no sample	no sample

References:

[1] J. Erlebacher, M.J. Aziz, A. Karma, N. Dimitrov, K. Sieradzki, Evolution of nanoporosity in dealloying, Nature. 410 (2001) 450–453. doi:10.1038/35068529.

[2] I. McCue, E. Benn, B. Gaskey, J. Erlebacher, Dealloying and Dealloyed Materials, Annu. Rev. Mater. Res. 46 (2016) 263–286. doi:10.1146/annurev-matsci-070115-031739.

[3] J. Weissmüller, K. Sieradzki, Dealloyed nanoporous materials with interface-controlled behavior, MRS Bull. 43 (2018) 14–19. doi:10.1557/mrs.2017.299.

[4] T. Fujita, P. Guan, K. McKenna, X. Lang, A. Hirata, L. Zhang, T. Tokunaga, S. Arai, Y. Yamamoto, N. Tanaka, Y. Ishikawa, N. Asao, Y. Yamamoto, J. Erlebacher, M. Chen, Atomic origins of the high catalytic activity of nanoporous gold, Nat. Mater. 11 (2012) 775–780. doi:10.1038/nmat3391.

[5] D. Kramer, R.N. Viswanath, J. Weissmüller, Surface-stress induced macroscopic bending of nanoporous gold cantilevers, Nano Lett. 4 (2004) 793–796. doi:10.1021/nl049927d.

[6] Q. Chen, Y. Ding, M. Chen, Nanoporous metal by dealloying for electrochemical energy conversion and storage, MRS Bull. 43 (2018) 43–48. doi:10.1557/mrs.2017.300.

[7] R. Li, K. Sieradzki, Ductile-brittle transition in random porous Au, Phys. Rev. Lett. 68 (1992) 1168–1171. doi:10.1103/PhysRevLett.68.1168.

[8] E. Detsi, M.S. Sellès, P.R. Onck, J.T.M. De Hosson, Nanoporous silver as electrochemical actuator, Scr. Mater. 69 (2013) 195–198. doi:10.1016/j.scriptamat.2013.04.003.

[9] S. Shi, J. Markmann, J. Weissmüller, Actuation by hydrogen electrosorption in hierarchical nanoporous palladium, Philos. Mag. 97 (2017) 1571–1587. doi:10.1080/14786435.2017.1311428.

[10] C. Cheng, L. Lührs, T. Krekeler, M. Ritter, J. Weissmüller, Semiordered Hierarchical Metallic Network for Fast and Large Charge-Induced Strain, Nano Lett. 17 (2017) 4774–4780. doi:10.1021/acs.nanolett.7b01526.

[11] T. Wada, H. Kato, Three-dimensional open-cell macroporous iron, chromium and ferritic stainless steel, Scr. Mater. 68 (2013) 723–726. doi:10.1016/j.scriptamat.2013.01.011.

[12] I.V. Okulov, A.V. Okulov, I.V. Soldatov, B. Luthringer, R. Willumeit-Römer, T. Wada, H. Kato, J. Weissmüller, J. Markmann, Open porous dealloying-based biomaterials as a novel biomaterial platform, Mater. Sci. Eng. C. 83 (2018) 95–103. doi:10.1016/j.msec.2018.03.008.

[13] M. Tsuda, T. Wada, H. Kato, Kinetics of formation and coarsening of nanoporous α-titanium dealloyed with Mg melt, J. Appl. Phys. 114 (2013). doi:10.1063/1.4821066.

[14] I.V. Okulov, A.V. Okulov, A.S. Volegov, J. Markmann, Tuning microstructure and mechanical properties of open porous TiNb and TiFe alloys by optimization of dealloying parameters, Scr. Mater. 154 (2018) 68–72. doi:10.1016/j.scriptamat.2018.05.029.

[15] T. Wada, A.D. Setyawan, K. Yubuta, H. Kato, Nano- to submicro-porous β-Ti alloy prepared from dealloying in a metallic melt, Scr. Mater. 65 (2011) 532–535. doi:10.1016/j.scriptamat.2011.06.019.

[16] T. Wada, K. Yubuta, A. Inoue, H. Kato, Dealloying by metallic melt, Mater. Lett. 65 (2011) 1076–1078. doi:10.1016/j.matlet.2011.01.054.

[17] I.P. Jain, C. Lal, A. Jain, Hydrogen storage in Mg: A most promising material, Int. J. Hydrogen Energy. 35 (2010) 5133–5144. doi:10.1016/j.ijhydene.2009.08.088.

[18] R. Mohtadi, F. Mizuno, Magnesium batteries: Current state of the art, issues and future perspectives, Beilstein J. Nanotechnol. 5 (2014) 1291–1311. doi:10.3762/bjnano.5.143.

[19] M.Q. Cheng, T. Wahafu, G.F. Jiang, W. Liu, Y.Q. Qiao, X.C. Peng, T. Cheng, X.L. Zhang, G. He, X.Y. Liu, A novel open-porous magnesium scaffold with controllable microstructures and properties for bone regeneration, Sci. Rep. 6 (2016) 1–14. doi:10.1038/srep24134.

[20] C.A. Volkert, E.T. Lilleodden, D. Kramer, J. Weissmüller, Approaching the theoretical strength in nanoporous Au, Appl. Phys. Lett. 89 (2006) 87–90. doi:10.1063/1.2240109.

[21] J. Biener, A.M. Hodge, J.R. Hayes, C.A. Volkert, L.A. Zepeda-Ruiz, A. V. Hamza, F.F. Abraham, Size effects on the mechanical behavior of nanoporous Au, Nano Lett. 6 (2006) 2379–2382. doi:10.1021/nl061978i.

[22] T. Zhang, Z. Tao, J. Chen, Magnesium–air batteries: from principle to application, Mater. Horiz. 1 (2014) 196–206. doi:10.1039/C3MH00059A.

[23] A. Kucharczyk, K. Naplocha, J.W. Kaczmar, H. Dieringa, K.U. Kainer, Current Status and Recent Developments in Porous Magnesium Fabrication, Adv. Eng. Mater. 1700562 (2017) 1–16. doi:10.1002/adem.201700562.

[24] I. McCue, B. Gaskey, P.A. Geslin, A. Karma, J. Erlebacher, Kinetics and morphological evolution of liquid metal dealloying, Acta Mater. 115 (2016) 10–23. doi:10.1016/j.actamat.2016.05.032.

[25] P. Geslin, I. Mccue, J. Erlebacher, A. Karma, Topology-generating interfacial pattern formation during liquid metal dealloying, Nat. Commun. 6 (2015) 1–19. doi:10.1038/ncomms9887.
[26] K.Y. Chiu, M.H. Wong, F.T. Cheng, H.C. Man, Characterization and corrosion studies of fluoride conversion coating on degradable Mg implants, Surf. Coatings Technol. 202 (2007) 590–598. doi:10.1016/j.surfcoat.2007.06.035.
[27] I.V. Okulov, M. Bönisch, U. Kühn, W. Skrotzki, J. Eckert, Significant tensile ductility and toughness in an ultrafine-structured Ti68.8Nb13.6Co6Cu5.1Al6.5 bi-modal alloy, Mater. Sci. Eng. A. 615 (2014) 457–463. doi:10.1016/j.msea.2014.07.108.
[28] I.V. Okulov, S. Pauly, U. Kühn, P. Gargarella, T. Marr, J. Freudenberger, L. Schultz, J. Scharnweber, C.-G. Oertel, W. Skrotzki, J. Eckert, Effect of microstructure on the mechanical properties of as-cast Ti–Nb–Al–Cu–Ni alloys for biomedical application, Mater. Sci. Eng. C. 33 (2013) 4795–4801. doi:10.1016/j.msec.2013.07.042.
[29] I.V. Okulov, M. Bönisch, A.V. Okulov, A.S. Volegov, H. Attar, M. Calin, S. Ehtemam-Haghighi, Z. Wang, A. Hohenwarter, I. Kaban, K.G. Prashanth, J. Eckert, Phase formation, microstructure and deformation behavior of heavily alloyed TiNb- and TiV-based titanium alloys, Mater. Sci. Eng. A. 732 (2018).
[30] C. Suryanarayana, A. Inoue, Bulk Metallic Glasses, CRC Press Taylor & Francis Group, 2011.
[31] C. Leyens, M. Peters, Titanium and Titanium Alloys, WILEY-VCH Verlag GmbH & Co. KGaA, Weinheim, 2003.
[32] I.V. Okulov, H. Wendrock, A.S. Volegov, H. Attar, U. Kühn, W. Skrotzki, J. Eckert, High strength beta titanium alloys: New design approach, Mater. Sci. Eng. A. 628 (2015) 297–302. doi:10.1016/j.msea.2015.01.073.
[33] I.V. Okulov, M. Bönisch, A.S. Volegov, H. Shahabi Shakur, H. Wendrock, T. Gemming, J. Eckert, Micro-to-nano-scale deformation mechanism of a Ti-based dendritic-ultrafine eutectic alloy exhibiting large tensile ductility, Mater. Sci. Eng. A. 682 (2017) 673–678. doi:10.1016/j.msea.2016.11.082.
[34] I.V. Okulov, M.F. Sarmanova, A.S. Volegov, A. Okulov, U. Kühn, W. Skrotzki, J. Eckert, Effect of boron on microstructure and mechanical properties of multicomponent titanium alloys, Mater. Lett. 158 (2015) 111–114. doi:10.1016/j.matlet.2015.06.017.
[35] H. Baker, ed., ASM Handbook: Alloy Phase Diagrams, ASM International, Materials Park, 1992.
[36] G.F. Vander Voort, ed., ASM Handbook: Metallography and Microstructures, ASM International, 2004.
[37] A.V. Okulov, A.S. Volegov, J. Weissmüller, J. Markmann, I.V. Okulov, Dealloying-based metal-polymer composites for biomedical applications, Scr. Mater. 146 (2018) 290–294. doi:10.1016/j.scriptamat.2017.12.022.
[38] Q. Chen, K. Sieradzki, Spontaneous evolution of bicontinuous nanostructures in dealloyed Li-based systems, Nat. Mater. 12 (2013) 1102–1106. doi:10.1038/nmat3741.
[39] J. Muldoon, C.B. Bucur, A.G. Oliver, T. Sugimoto, M. Matsui, H.S. Kim, G.D. Allred, J. Zajicek, Y. Kotani, Electrolyte roadblocks to a magnesium rechargeable battery, Energy Environ. Sci. 5 (2012) 5941. doi:10.1039/c2ee03029b.
[40] I. V Okulov, J. Weissmüller, J. Markmann, Dealloying-based interpenetrating-phase nanocomposites matching the elastic behavior of human bone, Sci. Rep. 7 (2017) 20. doi:10.1038/s41598-017-00048-4.

Acknowledgements

I.V.O. thanks Prof. Geslin, Prof. Joo, and Mrs. Sarmanova for valuable discussions. Funding by the Helmholtz Impuls- und Vernetzungsfonds via the Helmholtz - Chinese Academy of Sciences Joint Research Group “Nanoporous transition metals for strength and function – towards a cost-efficient materials base” grant no. HCJRG-315 and by the International Collaboration Center, Institute for Materials Research (ICC-IMR), Tohoku University, Japan are gratefully acknowledged.

Author Contributions

I.V.O. designed and performed experiments on dealloying; I.V.O. and S.V.L. designed and performed experiments on etching; I.V.O. and S.V.L. characterized samples and analyzed data; T.W. performed FIB; K.Y. performed TEM; I.V.O. wrote the manuscript; all authors discussed the results and contributed to the manuscript.

Notes

The authors declare no competing financial interest.

View publication stats